

## Article

# Fluorescence Enhancement via Dual Coupling of Dye Molecules with Silver Nanostructures

Vien Thi Tran <sup>1,2</sup>  and Heongkyu Ju <sup>1,2,\*</sup> <sup>1</sup> Department of Physics, Gachon University, Seongnam-si 13120, Gyeonggi-do, Korea; tranvien04@gmail.com<sup>2</sup> Gachon Bionano Research Institute, Seongnam-si 13120, Gyeonggi-do, Korea

\* Correspondence: batu@gachon.ac.kr; Tel.: +82-31-750-8552

**Abstract:** We demonstrate the enhancement of fluorescence emitted from dye molecules coupled with two surface plasmons, i.e., silver nanoparticles (AgNPs)-induced localized surface plasmons (LSP) and thin silver (Ag) film supported surface plasmons. Excitation light is illuminated to a SiO<sub>2</sub> layer that contains both rhodamine 110 molecules and AgNPs. AgNPs enhances excitation rates of dye molecules in their close proximity due to LSP-induced enhancement of local electromagnetic fields at dye excitation wavelengths. Moreover, the SiO<sub>2</sub> layer on one surface of which a 50 nm-thick Ag film is coated for metal cladding (air on the other surface), acts as a waveguide core at the dye emission wavelengths. The Ag film induces the surface plasmons which couple with the waveguide modes, resulting in a waveguide-modulated version of surface plasmon coupled emission (SPCE) for different SiO<sub>2</sub> thicknesses in a reverse Kretschmann configuration. We find that varying the SiO<sub>2</sub> thickness modulates the fluorescent signal of SPCE, its modulation behavior being in agreement with the theoretical simulation of thickness dependent properties of the coupled plasmon waveguide resonance. This enables optimization engineering of the waveguide structure for enhancement of fluorescent signals. The combination of LSP enhanced dye excitation and the waveguide-modulated version of SPCE may offer chances of enhancing fluorescent signals for a highly sensitive fluorescent assay of biomedical and chemical substances.

**Keywords:** surface plasmon coupled emission; waveguide; localized surface plasmon; fluorescence enhancement; metal nanostructures



**Citation:** Tran, V.T.; Ju, H. Fluorescence Enhancement via Dual Coupling of Dye Molecules with Silver Nanostructures. *Chemosensors* **2021**, *9*, 217. <https://doi.org/10.3390/chemosensors9080217>

Academic Editors: Iole Venditti, Paolo Proposito and Alessandra Paladini

Received: 29 June 2021  
Accepted: 9 August 2021  
Published: 10 August 2021

**Publisher's Note:** MDPI stays neutral with regard to jurisdictional claims in published maps and institutional affiliations.



**Copyright:** © 2021 by the authors. Licensee MDPI, Basel, Switzerland. This article is an open access article distributed under the terms and conditions of the Creative Commons Attribution (CC BY) license (<https://creativecommons.org/licenses/by/4.0/>).

## 1. Introduction

Plasmonic metal nanostructures have been intensively explored due to their intrinsic features of the local fields enhancement for strengthened interaction between light and electronic dipoles that scatter or fluoresce. This enhanced interaction may find use in a wide variety of applications across a linear-nonlinear optics boundary, such as plasmonic nanolenses [1,2], photothermal therapy [3,4], super-continuum generation of light [5,6], surface enhanced Raman spectroscopy [7,8], highly efficient harvest of solar energy [9,10], high-resolution imaging [11,12], label-free optical bio-environmental sensors [13–15], and metal-enhanced fluorescence-based diagnosis of biomedical and chemical molecules [16–19].

Fluorescence, in general, inherently suffers from photo-bleaching and restricted efficiency in collecting all-direction radiated fluorescent light, but these issues can be circumvented via tailoring of plasmonic local fields around dye molecules. Metal nanostructures such as thin metal films can also support the surface plasmon coupled emission (SPCE) of fluorophores that occurs via the non-radiative decay channel of the excited dye molecules into surface plasmons through near field interaction in a reverse Kretschmann configuration [18,20,21]. This in turn reradiates the far-field light into a high refractive index medium as it is p-polarized through the metal film at specific angles at the emission wavelengths ( $\lambda_{em}$ ). Overall, this leads to an enhanced energy transfer from the excitation light source at the excitation wavelengths ( $\lambda_{ex}$ ) to the emission channel at  $\lambda_{em}$  with a highly directional nature of emission radiation that greatly favors the light collection efficiency [22,23]. SPCE

eventually results in a net enhancement of detected fluorescence alongside an additional benefit, i.e., the reduction of photo-bleaching [24].

It was reported that the properties of the SPCE (in a reverse Kretschmann configuration) relied on the thickness of the polyvinyl alcohol (PVA) layer that contained dye molecules, coated on a 50 nm silver (Ag) film. Variation of the thickness changed SPCE angle and its polarizations at  $\lambda_{em}$ , as interpreted due possibly to thickness-dependent waveguide modes propagating along the layer [25].

It was also found that surface plasmons (SP) coupled with waveguide modes in the Kretschmann configurations [26–28]. One of the waveguide coupled modes, the so-called coupled plasmon waveguide resonance (CPWR) [25,29–33], is expected to offer the high quality factor of surface plasmon oscillation with extended penetration depth of the evanescent fields into a dielectric side at an appropriate waveguide core thickness.

Meanwhile, the interaction of light with a metal nanoparticle with its diameter much smaller than the wavelength, leads to the localized surface plasmon resonance (LSPR). LSPR produces the local fields greatly enhanced around the nanoparticles, offering the photonic mode density extraordinarily high in the nanometric volume of space near around the particle surface. Metal nanoparticles have been utilized to generate hot spots to enhance the excitation rates of fluorescent dye molecules [34] or for de-quenching SPCE when combined with a thin metal film to form nano-gap junction [35].

In this paper, we report an approach of combining LSP-induced enhanced excitation of dye molecules and the waveguide-surface plasmon coupling at dye emission wavelengths for waveguide-modulated SPCE. This dual coupling of dye molecules with surface plasmons at both  $\lambda_{ex}$  and  $\lambda_{em}$  leads to a fluorescence enhancement. Ag nanoparticles (AgNP)s embedded in a rhodamine 110 containing SiO<sub>2</sub> layer induces LSPR for enhancing the dye excitation rates at  $\lambda_{ex}$ . The SiO<sub>2</sub> layer on one surface of which a 50 nm-thick Ag film is coated for a metal cladding [36] (air cladding on the other surface), acts as a waveguide core. This enables SPCE to be coupled with waveguide modes at  $\lambda_{em}$  in a reverse Kretschmann configuration, corresponding to CPWR in a Kretschmann configuration (at  $\lambda_{em}$ ).

Varying the SiO<sub>2</sub> layer thickness can modulate the fluorescent signal of SPCE, leading to its optimization at its appropriate thickness where the surface plasmon-dye coupling strength is maximized. We find that the thickness dependence of the fluorescent signal of SPCE qualitatively follows that of the depth-to-width ratio ( $\Gamma$ ) of the reflectance dip in a Kretschmann configuration that uses the SiO<sub>2</sub> layer for CPWR. Considering such  $\Gamma$  as proportional to quality factor of surface plasmons [37], this feature enables the SiO<sub>2</sub> thickness-dependent fluorescent signal of SPCE to be interpreted as due largely to thickness-dependent interaction of excited dye molecules with surface plasmons whose evanescent fields strength into the SiO<sub>2</sub> layer is thickness-dependent at  $\lambda_{em}$ .

Combining an LSP-induced increase in excitation rate and waveguide-enhanced SPCE for fluorescent signal optimization may find use in fluorescence spectroscopy for a highly sensitive assay of biomedical and chemical substances.

## 2. Experimental Section

### 2.1. Fabrication of the Plasmonic Chip for Fluorescence Enhancement

A plasmonic fluorescence chip is fabricated by depositing a 50 nm-thick Ag film (Ag: 99.99%, iTASCO, Seoul, Korea) and a 10 nm-thick MgF<sub>2</sub> layer (MgF<sub>2</sub>: 99%, iTASCO, Seoul, Korea) consecutively on a slide glass of an area of 15 × 15 mm<sup>2</sup> (Marienfeld, Cologne, Germany) using a thermal evaporator system (DAEKI-TECH Co., Ltd., Daejeon, Korea). We take the Ag film thickness to be 50 nm which would produce optimized  $\Gamma$  of the calculated reflectance dip in a typical angle-interrogated Kretschmann configuration at  $\lambda_{em}$ , to optimize surface plasmon resonance (SPR) quality factor (see Figure S1 in the Supplementary Materials). This Ag film thickness in a reverse Kretschmann configuration (currently presented) is also expected to optimize the quality factor of the surface plasmons that couple with excited dye molecules at  $\lambda_{em}$ .

We coat a 10 nm-thick MgF<sub>2</sub> layer on the Ag film to hinder possible quenching of dye molecules in a close proximity to the Ag film (quenching results from a non-radiative decay of dye molecules into the metal film such as the Förster resonance energy transfer) [38,39].

A waveguide core layer that contains dye molecules is spin-coated on the MgF<sub>2</sub> layer as follows: The silica (SiO<sub>2</sub>) precursor sol-gel is made of tetraethyl orthosilicate (TEOS, 98%, Sigma, Ronkonkoma, NY, USA), ethanol (98%, Sigma, Ronkonkoma, NY, USA), deionized water (Biosesang, Seongnam, Korea), and hydric acid (HCl, 37%, Sigma, Ronkonkoma, NY, USA) with the respective molar ratio of 1:10:2:0.0037. In the first place, the first three constituents are mixed and stirred for 30 min. We then add HCl to it and stir the mixture again for 3 h. We then add the sodium hydroxide (NaOH, Sigma, Ronkonkoma, NY, USA) of 0.05 M for catalytic sol-gel reaction and again stir the mixture for 16 h to obtain the SiO<sub>2</sub> precursor. Meanwhile, we dissolve the rhodamine 110 (Rho110, 99%, Sigma, Ronkonkoma, NY, USA) powder in ethanol solvent. Then, we mix the dye solution with the SiO<sub>2</sub> precursor to fabricate the dye-embedded SiO<sub>2</sub> layer (waveguide core) through a spin-coating technique.

Prior to spin-coating, the surface of the MgF<sub>2</sub> layer is modified into a hydrophilic one by oxygen plasma treatment (Cute, Femtoscience, Hwaseong, Korea) for 2 min with O<sub>2</sub> gas of 15 sccm. A spin coater (ACE-200, Dong Ah, Seoul, Korea) is used to deposit the dye solution-SiO<sub>2</sub> precursor mixture of 30 µL volume two times in a row, i.e., with 300 rpm for 10 s and with 2600 rpm for 50 s. We then dry the coated layer in an oven at 60 °C for 30 min, into a solid form as the dye-embedded SiO<sub>2</sub> layer.

We vary the thickness of the SiO<sub>2</sub> layer by increasing the volumetric portion of the SiO<sub>2</sub> precursor in a given mixture of 30 µL volume, i.e., from 20% (6 µL) to 50% (15 µL) by steps of 10% with a consequence of thicknesses of 141 ± 8 nm, 159 ± 7 nm, 199 ± 1 nm, and 259 ± 4 nm. An atomic force microscope (Veeco Metrology system, Model No. 920-006-101) is used to determine the thicknesses in the step-height mode.

For coating the SiO<sub>2</sub> layer that has both AgNPs and dye molecules embedded in it, we add AgNPs with their average diameters of 75 nm (nanoComposix, Co., Ltd., San Diego, CA, USA) to the mixture comprised of a SiO<sub>2</sub> precursor prior-mixed with dye solution mentioned above. The particle concentration is 0.125 mg/mL. We spin-coat a SiO<sub>2</sub> layer out of this mixture onto the MgF<sub>2</sub> surface. The dimension of the fabricated chips is shown in Figure 1a.

Figure 1(b1–b4) illustrates the four kinds of chips fabricated for comparison in the fluorescence detection. Figure 1(b1) depicts the chip structure that produces fluorescence from rhodamine 110 molecules within the SiO<sub>2</sub> layer. This chip is expected to produce fluorescence unaffected by surface plasmons induced by the Ag film or AgNPs, i.e., the control fluorescence signal as the reference to be used for comparison with that of the other chips. Figure 1(b2) shows the structure for the fluorescence altered only by AgNPs embedded in the SiO<sub>2</sub> layer. Figure 1(b3) shows the chip structure whereby the dye involving SiO<sub>2</sub> layer acts as a waveguide core while both the Ag film and air act as cladding. The Ag film is used not only as a waveguide cladding but also as a plasmonic layer for waveguide-modulated SPCE in a reverse Kretschmann configuration. Finally, the chip structure for fluorescence modified by both AgNPs and waveguide-modulated SPCE is shown in Figure 1(b4).

Scanning electron microscope (SEM) images of the nearly smooth surface of the dye embedded SiO<sub>2</sub> layer supports the uniform dye dispersion in it, as shown in Figure S2a. The SEM image of the SiO<sub>2</sub> layer that has not only dye molecules but also AgNPs embedded in it shows distribution of a clustered pattern of AgNPs, as shown in Figure S2b. The fact that the inter-particle distance that varies in a certain range may affect the LSPR extinction spectrum into a broader one due to dipole–dipole interaction [40].

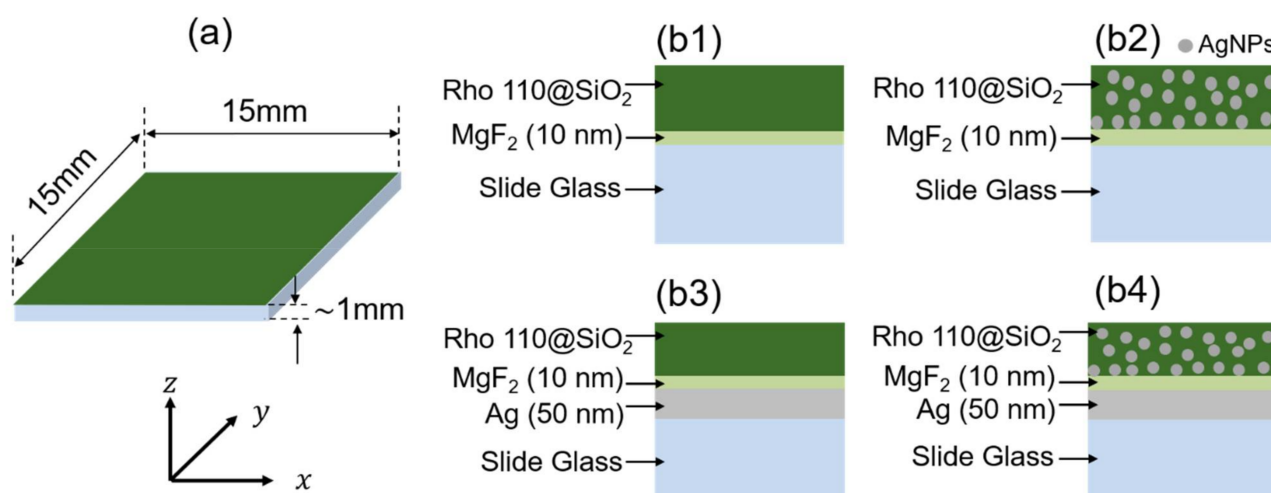


**Figure 1.** (a) The chip dimension; (b1–b4) schematic of the side views of the four different fluorescence chips used for fluorescence detection. Rho 110@SiO<sub>2</sub> represents the rhodamine 110 molecules dispersed within a SiO<sub>2</sub> layer. The structure in (b1) is used for control fluorescence signal.

Using a spectrometer (USB-2000, Ocean Optics, Orlando, FL, USA), we measured the emission spectrum of the rhodamine 110 embedded in the SiO<sub>2</sub> layer under illumination of dye excitation light of a LED centered at 470 nm wavelength (M470L3, Thorlabs, Newton, MA, USA). A spectrum of the emission wavelength peaks at 517 nm are shown by the green solid curve in Figure 2. This confirmed the fact that the emission spectrum is subject to the ambient medium (SiO<sub>2</sub>) around the dye molecules, given the fact that its peak occurs at 520 nm when they are in an ethanol solvent [41].

A LSPR extinction spectrum of light due to AgNPs embedded in the SiO<sub>2</sub> layer is measured using a UV-Vis spectrophotometer (Varian Cary 50, Santa Clara, CA, USA) with its peak at 484 nm as shown by black dashed curve in Figure 2. The broadened spectrum of LSPR extinction with its peak wavelength close to the dye excitation spectrum peak (498 nm) could offer the substantial spectral overlapping between LSPR extinction and dye excitation spectra.

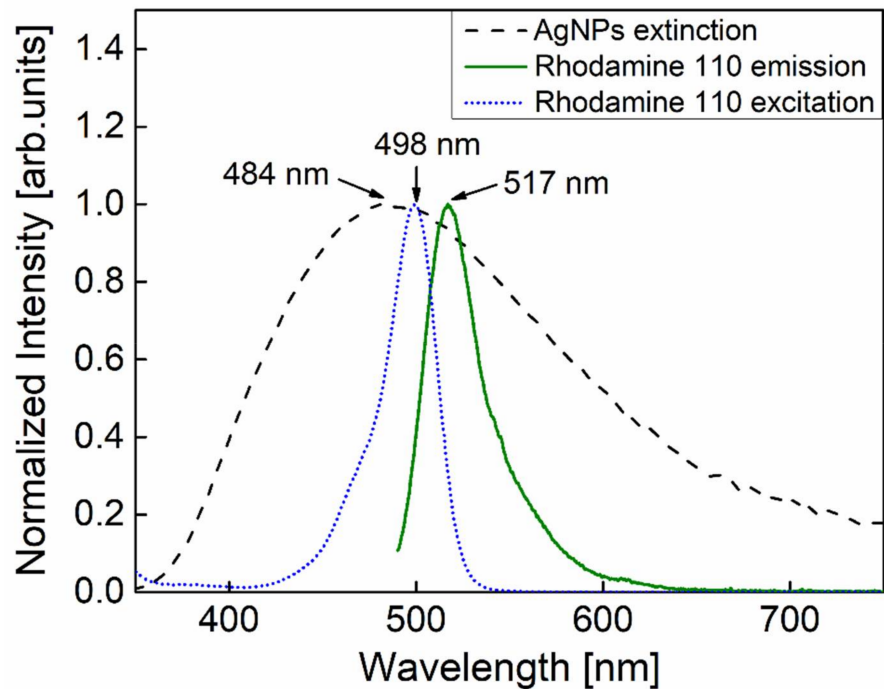
## 2.2. Fluorescence Detection System

Figure 3a illustrates a schematic of the setup used for detecting optical power of SPCE induced directional radiation, where a LED (centered at 470 nm) is used to excite rhodamine 110 molecules. The LED light spectrally filtered by an excitation filter (EXF) ( $470 \pm 20$  nm, Chroma Technology, Bellows Falls, VT, USA) illuminates the fluorescence chip surface through an iris that controls the illumination area. The optical power incident to the chip surface is 17 mW. While part of the fluorescence would then emit back into air, the SPCE can produce directional radiation into a N-BK7 prism at a specific angle  $\theta_s$  as shown in Figure 3a.

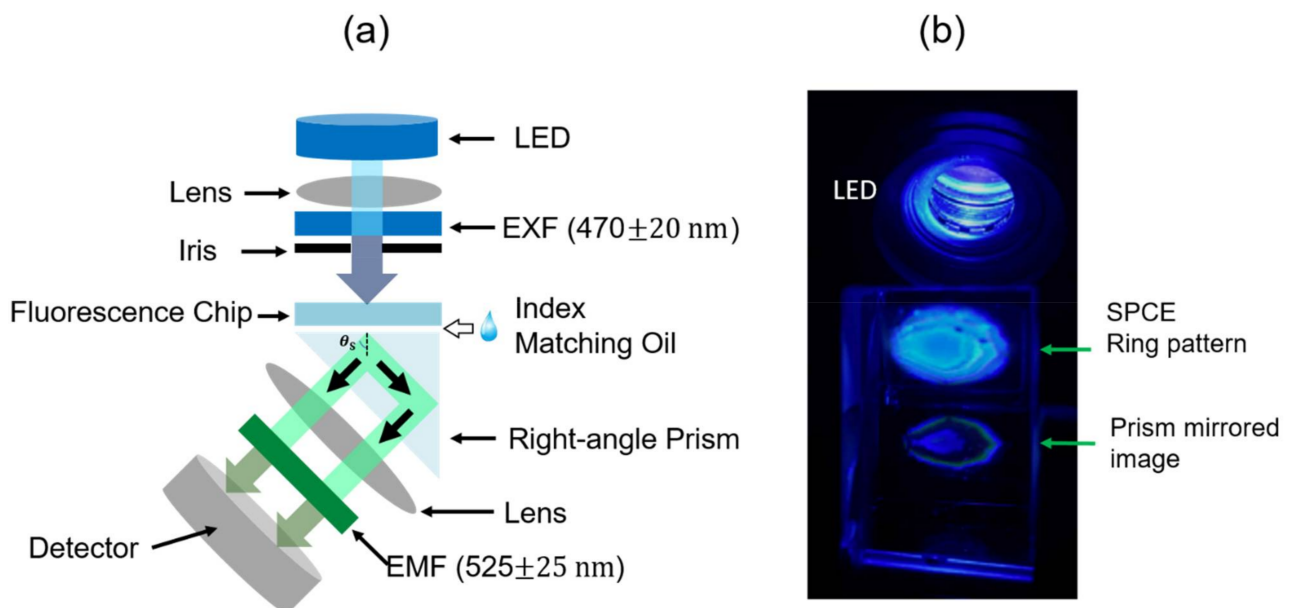
We minimize the chip-prism index discontinuity with the matching oil index inserted in between. The prism that acts as an internal reflector collects the SPCE light, considering the SPCE angle that ranges from 40° to 45° for different thicknesses of the chip SiO<sub>2</sub> layer, with a given critical angle  $\sim 41^\circ$  of total internal reflection at the prism-air interface. The subsequent lens then gathers the prism-collected light into a photomultiplier tube (PMT) (PMM02, Thorlabs, Newton, MA USA). We place an emission spectral filter (EMF) ( $525 \pm 25$  nm), Chroma Technology, Atlanta, GA, USA just prior to the PMT to allow optical power only at  $\lambda_{em}$  to be detected while suppressing that at  $\lambda_{ex}$ .

Figure 3b shows a photo of the ring patterns of fluorescence emission, taken at the PMT position where a camera is tilted to face the prism base surface. This results from the SPCE-induced conical radiation of a given angle  $\theta_s$ . Part of the prism-coupled emission

directly reaches the detector, whereas others do so after reflection off the prism side surface with a result of the mirrored image as shown by the second ring patterns in Figure 3b.



**Figure 2.** A rhodamine 110 excitation spectrum (blue dotted curve) is taken from the dye manufacturer data. The green solid curve and black dashed curve represent the measured spectra of fluorescence emitting from rhodamine 110 dispersed within a SiO<sub>2</sub> layer, and the LSPR-induced extinction due to the AgNPs embedded within the layer, respectively.



**Figure 3.** (a) Schematic of a setup for fluorescence detection. (EXF: excitation filter, EMF: emission filter,  $\theta_s$ : the angle for SPCE). (b) A photo of the ring patterns of emission coupled into the prism, taken from the PMT position at an angle tilted to face the prism base surface. The ring pattern image mirrored from the prism side is seen below the main ring pattern.

Appropriate signal analysis should take into account the background signal mainly due to the optical power leaking through the EMF at  $\lambda_{ex}$  and broadband dark noise. A substantial amount of these noise signals including auto-fluorescence can be removed by subtracting the signal measured with the corresponding blank chip (zero dye concentration) from that measured with the chip of a given nonzero dye concentration. This provides the net signal produced solely due to that arising from dye emission at  $\lambda_{em}$ . Error bars are obtained by three independent chips for a given  $\text{SiO}_2$  thickness for each structure of the four different types of chips while single shot measurement lasts 10 s with 1 Hz sampling record frequency with a PMT-connected multimeter.

### 3. Result and Discussion

Figure 4 shows the net fluorescent signals (dark solid triangles) detected with the chip of Figure 1(b2) in comparison with control signals (dark empty squares) detected with the chip of Figure 1(b1) installed in the setup of Figure 3a. Use of AgNPs enhances the net fluorescent signal over the control counterpart at each  $\text{SiO}_2$  thickness due to enhancement of the dye excitation rate by AgNPs-induced LSPR. Moreover, non-negligible dependence of the net signal on  $\text{SiO}_2$  thickness is found despite the fact that all the  $\text{SiO}_2$  layers of the four different thickness involve the same number of dye molecules and AgNPs. However, it is unclear how the thickness of  $\text{SiO}_2$  layer involving dye molecules and AgNPs, affects the LSPR induced enhancement of excitation rates to explain such thickness dependence.

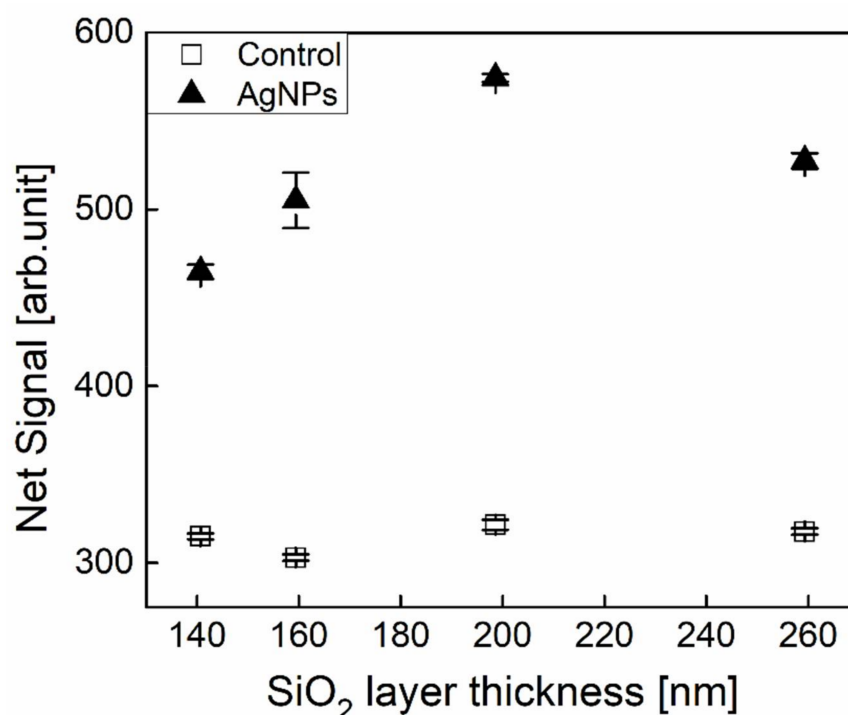


**Figure 4.** Net fluorescence signals obtained using the chips of Figure 1(b2) installed in the setup of Figure 3a. The thicknesses of the  $\text{SiO}_2$  layer wherein rhodamine 110 molecules were dispersed were 141, 159, 199, and 259 nm. Error bar =  $\pm\text{SD}$ ,  $n = 3$ .

Use of the 50 nm-thick Ag film within the chip as shown in Figure 1(b3) produces SPCE in a reverse Kretschmann configuration, as a result of near field coupling of excited dye molecules with the metallic film into surface plasmons at  $\lambda_{em}$ . The net fluorescent signal clearly exhibits the  $\text{SiO}_2$  thickness dependence, with its maximum occurring at 199 nm, as shown by black solid circles in Figure 5a. This thickness dependence can be accounted for by  $\text{SiO}_2$  thickness-induced modulation of strength of coupling between

excited dye molecules and the thin metallic film, which can be represented by strength of the evanescent field of resultant surface plasmons at  $\lambda_{em}$ .

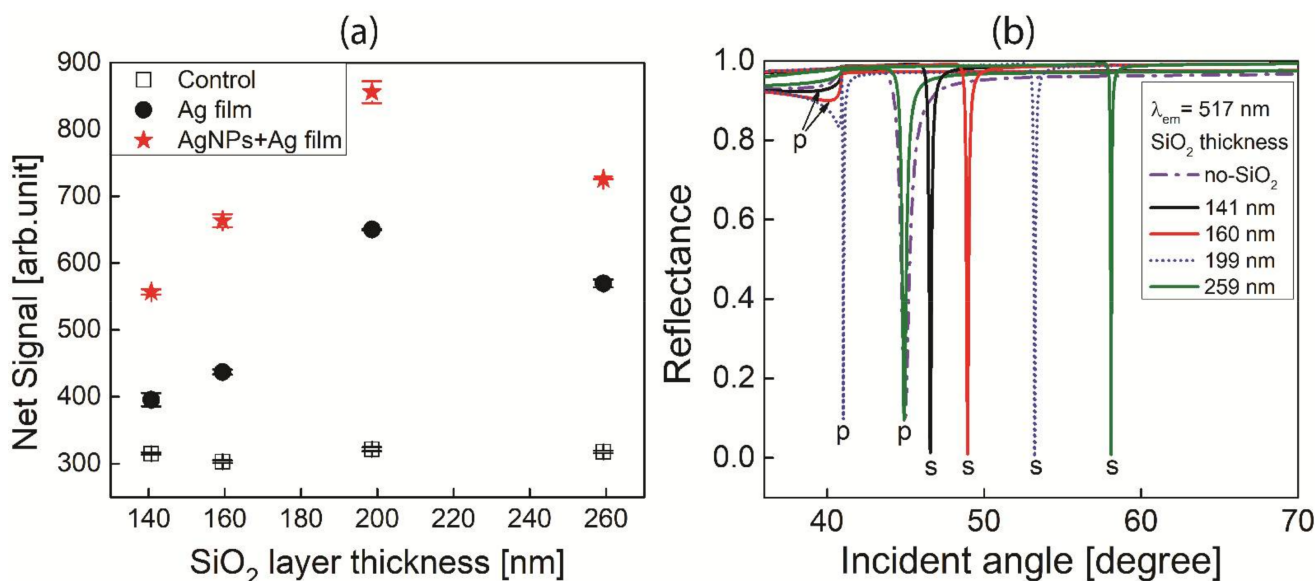


**Figure 5.** (a) Net signals obtained from measurement setup of Figure 3a at wavelengths of  $525 \pm 25$  nm using the four different chips seen in Figure 1(b3,b4). The thicknesses of the SiO<sub>2</sub> layer wherein rhodamine 110 molecules were dispersed were 141, 159, 199, and 259 nm. Error bar =  $\pm$ SD,  $n = 3$ . (b) Numerical simulation of reflectance versus incident angle in a Kretschmann configuration at  $\lambda_{em}$  for p- and s-polarizations that was assumed to have a SiO<sub>2</sub> layer/50 nm Ag film on its prism base. Optical parameters used for calculation are found in Section S3 in Supplementary Materials.

In order to understand such SiO<sub>2</sub> thickness dependence of surface plasmon evanescent field strength at  $\lambda_{em}$ , we numerically simulate the optical reflectance in an angle-interrogating Kretschmann configuration that encompasses a N-BK7 prism, on the base surface of which the layers of semi-infinite air/SiO<sub>2</sub> layer/50 nm-thick Ag film are assumed to be placed. In this setup, light is assumed to be incident on the prism at the SPR angle so its energy can be prism-coupled evanescently into the chip for the four different thicknesses of SiO<sub>2</sub> layers.

Figure 5b shows the calculated reflectance at 517 nm (fluorescence spectrum peak mentioned above) using a multi-layer transfer matrix approach with an optical parameter set given in Section S3 of Supplementary Materials for p- and s-polarizations. The SiO<sub>2</sub> thickness, in this case, governs the  $\Gamma$  of the reflectance dip, which is in proportion to the surface plasmon quality factor, as a result of waveguide-surface plasmon coupling, similarly reported as CPWR in [28,29]. Note that, for this calculation, use of the 50 nm-thick Ag film can support the surface plasmon generation for SPCE while simultaneously playing a role as a metal cladding for the SiO<sub>2</sub> waveguide core layer at 517 nm.

The SiO<sub>2</sub> thickness dependence of  $\Gamma$  manifests such coupling between waveguide and surface plasmons as seen in Figure 6 which shows the average of  $\Gamma$  over both polarizations at each SiO<sub>2</sub> thickness. The average  $\Gamma$  peaks at 199 nm while, for p- and s-polarizations,  $\Gamma$  peaks at the thickness of 199 and 259 nm, respectively as shown in inset of Figure 6. We find that the thickness dependence of the average  $\Gamma$  agrees qualitatively with that of the net fluorescent signal shown by black solid circles in Figure 5a. The waveguide-surface plasmon coupling can lead to larger  $\Gamma$  than the case of no SiO<sub>2</sub> layer. The SiO<sub>2</sub> layer thickness providing larger  $\Gamma$  due to CPWR, would lead to larger strength of the plasmonic evanescent fields penetrated into the SiO<sub>2</sub> layer in a Kretschmann configuration.

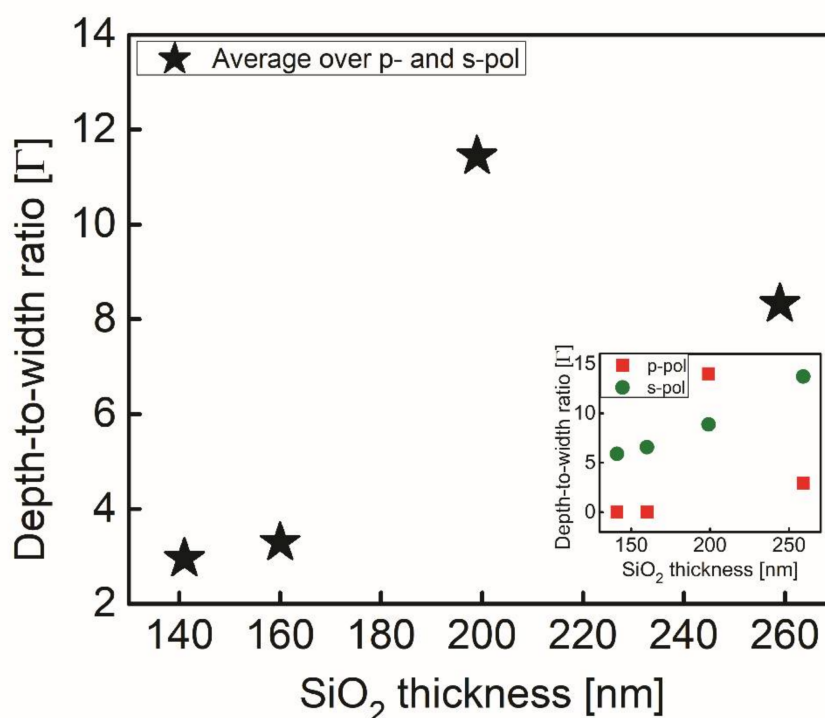


**Figure 6.** Average of depth-to-width ratio ( $\Gamma$ ) of the reflectance dip over two polarizations (p and s) at each SiO<sub>2</sub> thickness. Inset shows  $\Gamma$  for p- and s-polarizations at each SiO<sub>2</sub> thickness.

It is also noted that s-polarization would support CPWR modes [28,29] with a certain SiO<sub>2</sub> thickness dependence of  $\Gamma$  at  $\lambda_{em}$  in a Kretschmann configuration. Furthermore, in a reverse Kretschmann configuration, the presence of waveguide is known to induce the SPCE-like directional emission for s-polarization as well as p-polarization [22]. Therefore, the above-mentioned SiO<sub>2</sub> thickness dependence of strength of waveguide-surface plasmon coupling can account for the thickness-dependent fluorescent net signal (black solid circles in Figure 5a), as deriving from the thickness dependent waveguide-modulated SPCE.

The chip structure as depicted by Figure 1(b4) makes additional constructive effects of AgNPs-aided enhancement of the dye excitation rate for the fluorescent net signal produced by the waveguide-modulated SPCE, as shown by red solid stars in Figure 5a. The major dependence of the net signal on the SiO<sub>2</sub> thickness, in this case, would be driven by the thickness dependence of the waveguide-modulated SPCE, whether the dye molecule excitation rate is enhanced or not by the AgNPs LSPR. The fact that the chip including both the Ag film and AgNPs produces the signal larger than that having either of them at each SiO<sub>2</sub> layer thickness indicates that the combination of AgNPs LSPR-induced local field enhancement and the waveguide-modulated SPCE results in an increase in the net fluorescent signal.

The constructive dual coupling of dye molecules with the metal nanostructures at two distinct wavelengths,  $\lambda_{ex}$ , and  $\lambda_{em}$ , i.e., the coupling of dye molecules with AgNPs at  $\lambda_{ex}$  and that with the Ag-film for waveguide-modulated SPCE  $\lambda_{em}$ , is schematically illustrated in Figure 7. It occurs owing to the spectral overlap between AgNPs LSPR and the dye excitation, and to the spectral overlap between waveguide-modulated SPR and the dye emission.

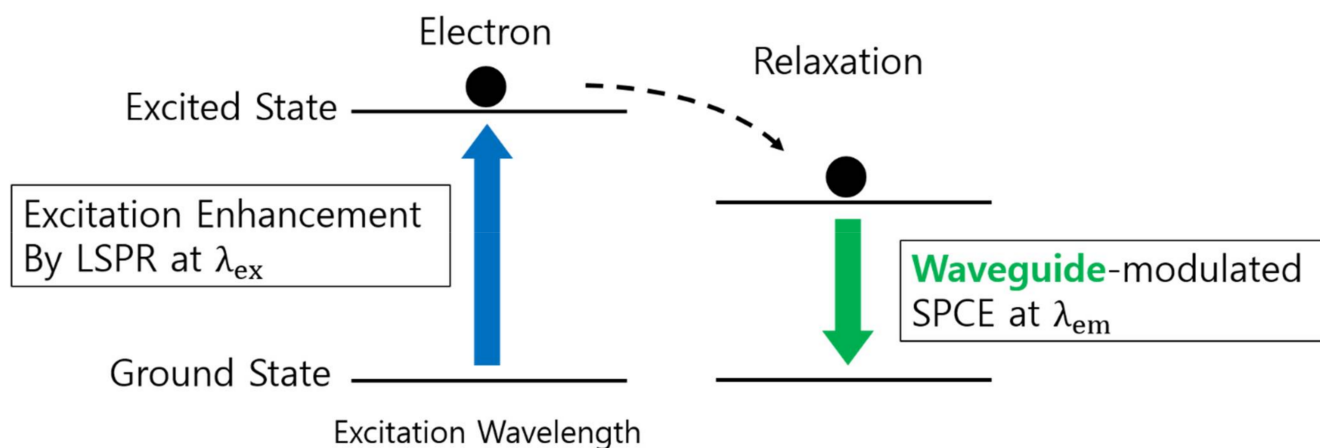


**Figure 7.** The dual coupling of dye molecules with the metal nanostructures, i.e., AgNPs, and the 50 nm-thick Ag film at two distinct wavelengths,  $\lambda_{ex}$ , and  $\lambda_{em}$ .

#### 4. Conclusions

We demonstrate the enhancement of fluorescence signal emitting from rhodamine 110 molecules using AgNPs-induced LSPR and waveguide-modulated SPCE. AgNPs embedded in a SiO<sub>2</sub> layer that also involves dye molecules enhances the dye excitation rates due to LSPR at  $\lambda_{ex}$ , provided that the LSPR spectrum significantly overlaps with the dye excitation spectrum. The SiO<sub>2</sub> layer bounded by both a 50 nm-thick Ag film and air acts as a waveguide core for light guiding at  $\lambda_{em}$ . Upon the spectral overlap between dye emission and SPR at  $\lambda_{em}$ , the waveguide structure enables excited dye molecules to couple with the thin metallic film for waveguide-modulated SPCE in a reverse Kretschmann configuration where the dye excitation light source of the LED is illuminated through air cladding. It is found that varying the SiO<sub>2</sub> thickness changes the net fluorescent signal detected as a result of the thickness-dependent waveguide-modulated SPCE. We find that the theoretical calculation of the SiO<sub>2</sub> thickness-dependent properties of surface plasmons associated with waveguide-modulated SPCE is in agreement with the measured fluorescent signal versus SiO<sub>2</sub> thickness.

One may achieve an increased enhancement factor of fluorescence via optimizing the AgNPs density and distribution in the SiO<sub>2</sub> layer. Though investigating the dye excitation source power and emission light collection optics, the current work focuses on the experimental feasibility of enhancing fluorescence by the dual coupling of dye molecules with localized surface plasmons at  $\lambda_{ex}$  and with waveguide-modulated surface plasmons for SPCE at  $\lambda_{em}$ .

Combining the AgNPs LSPR-enhanced dye excitation rate with the waveguide-modulated SPCE turns out to be constructive to the signal-to-noise ratio in the fluorescent signal. The combined technologies using the dual coupling of dye molecules with metal nanostructures may offer chances of enhancing fluorescent signals for a highly sensitive fluorescent assay of biomedical and chemical substances.

**Supplementary Materials:** The following are available online at <https://www.mdpi.com/article/10.3390/chemosensors9080217/s1>, Figure S1: The simulation of optical reflectance versus incident angle in a Kretschmann configuration with a thin Ag film coated prism. Figure S2: Scanning electron microscope (SEM) images for surface of a rhodamine 110 involving SiO<sub>2</sub> layer, Figure S3: the optical parameter set used for the optical reflection as a function of the incident angle in the Kretschmann configuration for Figure 5b.

**Author Contributions:** Conceptualization, H.J.; methodology, V.T.T.; software, V.T.T.; validation, V.T.T. and H.J.; formal analysis, V.T.T. and H.J.; investigation, V.T.T. and H.J.; resources, H.J.; data curation, V.T.T. and H.J.; writing—original draft preparation, V.T.T. and H.J.; writing—review and

editing, H.J.; visualization, V.T.T. and H.J.; supervision, H.J.; project administration, H.J.; funding acquisition, H.J. All authors have read and agreed to the published version of the manuscript.

**Funding:** This work was supported by the National Research Foundation of Korea (NRF) grant funded by the Korean government (MSIT) (No. 2020R1F1A1050885), and also supported by the Gachon University research fund of 2019 (GCU-2019-0803).

**Institutional Review Board Statement:** Not applicable.

**Informed Consent Statement:** Not applicable.

**Data Availability Statement:** The data presented in this study are available on request from the corresponding author. The data are not publicly available due to privacy.

**Conflicts of Interest:** The authors declare that they have no known competing financial interests or personal relationships that could have appeared to influence the work reported in this paper.

## References

1. Horton, M.J.; Ojambati, O.S.; Chikkaraddy, R.; Deacon, W.M.; Kongsuwan, N.; Demetriadou, A.; Hess, O.; Baumberg, J.J. Nanoscopy through a plasmonic nanolens. *Proc. Natl. Acad. Sci. USA* **2020**, *117*, 2275–2281. [[CrossRef](#)]
2. Biswas, S.; Liu, X.; Jarrett, J.W.; Brown, D.; Pustovit, V.; Urbas, A.; Knappenberger, K.L., Jr.; Nealey, P.F.; Vaia, R.A. Nonlinear Chiro-Optical Amplification by Plasmonic Nanolens Arrays Formed via Directed Assembly of Gold Nanoparticles. *Nano Lett.* **2015**, *15*, 1836–1842. [[CrossRef](#)]
3. Yuan, H.; Fales, A.M.; Vo-Dinh, T. TAT Peptide-Functionalized Gold Nanostars: Enhanced Intracellular Delivery and Efficient NIR Photothermal Therapy Using Ultralow Irradiance. *J. Am. Chem. Soc.* **2012**, *134*, 11358–11361. [[CrossRef](#)]
4. Aioub, M.; Panikkanvalappil, S.R.; El-Sayed, M.A. Platinum-Coated Gold Nanorods: Efficient Reactive Oxygen Scavengers That Prevent Oxidative Damage toward Healthy, Untreated Cells during Plasmonic Photothermal Therapy. *ACS Nano* **2017**, *11*, 579–586. [[CrossRef](#)]
5. Sivis, M.; Duwe, M.; Abel, B.; Ropers, C. Extreme-ultraviolet light generation in plasmonic nanostructures. *Nat. Phys.* **2013**, *9*, 304–309. [[CrossRef](#)]
6. Krasavin, A.V.; Ginzburg, P.; Wurtz, G.A.; Zayats, A.V. Nonlocality-driven supercontinuum white light generation in plasmonic nanostructures. *Nat. Commun.* **2016**, *7*, 11497. [[CrossRef](#)]
7. Kim, N.; Thomas, M.R.; Bergholt, M.S.; Pence, I.J.; Seong, H.; Charchar, P.; Todorova, N.; Nagelkerke, A.; Belessiotis-Richards, A.; Payne, D.J.; et al. Surface enhanced Raman scattering artificial nose for high dimensionality fingerprinting. *Nat. Commun.* **2020**, *11*, 207. [[CrossRef](#)]
8. Shiota, M.; Naya, M.; Yamamoto, T.; Hishiki, T.; Tani, T.; Takahashi, H.; Kubo, A.; Koike, D.; Itoh, M.; Ohmura, M.; et al. Gold-nanofève surface-enhanced Raman spectroscopy visualizes hypotaurine as a robust anti-oxidant consumed in cancer survival. *Nat. Commun.* **2018**, *9*, 1561. [[CrossRef](#)]
9. Carretero-Palacios, S.; Jimenez-Solano, A.; Míguez, H. Plasmonic Nanoparticles as Light-Harvesting Enhancers in Perovskite Solar Cells: A User's Guide. *ACS Energy Lett.* **2016**, *1*, 323–331. [[CrossRef](#)]
10. Cui, J.; Li, Y.; Liu, L.; Chen, L.; Xu, J.; Ma, J.; Fang, G.; Zhu, E.; Wu, H.; Zhao, L.; et al. Near-Infrared Plasmonic-Enhanced Solar Energy Harvest for Highly Efficient Photocatalytic Reactions. *Nano Lett.* **2015**, *15*, 6295–6301. [[CrossRef](#)]
11. Masuda, S.; Yanase, Y.; Usukura, E.; Ryuzaki, S.; Wang, P.; Okamoto, K.; Kuboki, T.; Kidoaki, S.; Tamada, K. High-resolution imaging of a cellattached nanointerface using a gold-nanoparticle two-dimensional sheet. *Sci. Rep.* **2017**, *7*, 3720. [[CrossRef](#)]
12. Williams, C.; Rughoobur, G.; Flewitt, A.J.; Wilkinson, T.D. Nanostructured plasmonic metapixels. *Sci. Rep.* **2017**, *7*, 7745. [[CrossRef](#)]
13. Kim, J.; Kim, S.; Nguyen, T.T.; Lee, R.; Li, T.; Yun, C.; Ham, Y.; An, S.S.A.; Ju, H. Label-free quantitative immunoassay of fibrinogen in Alzheimer disease patient plasma using fiber optical surface plasmon resonance. *J. Electron. Mater.* **2016**, *45*, 2354–2360. [[CrossRef](#)]
14. Tran, V.T.; Yoon, W.J.; Lee, J.-H.; Ju, H. DNA sequence-induced modulation of bimetallic surface plasmons in optical fibers for sub-ppq (parts-per-quadrillion) detection of mercury ions in water. *J. Mater. Chem. A* **2018**, *6*, 23894–23902. [[CrossRef](#)]
15. Kim, J.; Son, C.; Choi, S.; Yoon, W.J.; Ju, H. A plasmonic fiber-based glucometer and its temperature dependence. *Micromachines* **2018**, *9*, 506. [[CrossRef](#)]
16. Choi, J.-H.; Choi, J.-W. Metal-Enhanced Fluorescence by Bifunctional Au Nanoparticles for Highly Sensitive and Simple Detection of Proteolytic Enzyme. *Nano Lett.* **2020**, *20*, 7100–7107. [[CrossRef](#)]
17. Fothergill, S.M.; Joyce, C.; Xie, F. Metal enhanced fluorescence biosensing: From ultra-violet towards second near-infrared window. *Nanoscale* **2018**, *10*, 20914–20929. [[CrossRef](#)]
18. Tran, N.H.T.; Trinh, K.T.L.; Lee, J.-H.; Yoon, W.J.; Ju, H. Reproducible Enhancement of Fluorescence by Bimetal Mediated Surface Plasmon Coupled Emission for Highly Sensitive Quantitative Diagnosis of Double-Stranded DNA. *Small* **2018**, *14*, 1801385. [[CrossRef](#)]

19. Tran, V.T.; Ju, H. Fluorescence Based on Surface Plasmon Coupled Emission for Ultrahigh Sensitivity Immunoassay of Cardiac Troponin I. *Biomedicines* **2021**, *9*, 448. [[CrossRef](#)]
20. Gryczynski, I.; Malicka, J.; Gryczynski, Z.; Lakowicz, J.R. Surface Plasmon-Coupled Emission with Gold Films. *J. Phys. Chem. B* **2004**, *108*, 12568–12574. [[CrossRef](#)]
21. Badugu, R.; Szmajcinski, H.; Ray, K.; Descrovi, E.; Ricciardi, S.; Zhang, D.; Chen, J.; Huo, Y.; Lakowicz, J.R. Metal–Dielectric Waveguides for High-Efficiency Coupled Emission. *ACS Photonics* **2015**, *2*, 810–815. [[CrossRef](#)]
22. Geddes, C.D.; Gryczynski, I.; Malicka, J.; Gryczynski, Z.; Lakowicz, J.R. Directional Surface Plasmon Coupled Emission. *J. Fluoresc.* **2004**, *14*, 119–123. [[CrossRef](#)]
23. Meng, L.; Yang, Z. Directional surface plasmon-coupled emission of tilted-tip enhanced spectroscopy. *Nanophotonics* **2018**, *7*, 1325–1332. [[CrossRef](#)]
24. Lakowicz, J.R.; Malicka, J.; Gryczynski, I.; Gryczynski, Z. Directional surface plasmon-coupled emission: A new method for high sensitivity detection. *Biochem. Biophys. Res. Commun.* **2003**, *307*, 435–439. [[CrossRef](#)]
25. Gryczynski, I.; Malicka, J.; Nowaczyk, K.; Gryczynski, Z.; Lakowicz, J.R. Effects of Sample Thickness on the Optical Properties of Surface Plasmon-Coupled Emission. *J. Phys. Chem. B* **2004**, *108*, 12073–12083. [[CrossRef](#)]
26. Kovacs, G.J.; Scott, G.D. Optical excitation of surface plasma waves in layered media. *Phys. Rev. B* **1977**, *16*, 1297. [[CrossRef](#)]
27. Kovacs, G.J.; Scott, G.D. Attenuated total reflection angular spectra and associated resonant electromagnetic oscillations of a dielectric slab bounded by Ag films. *Appl. Opt.* **1978**, *17*, 3314–3322. [[CrossRef](#)] [[PubMed](#)]
28. Chyou, J.-J.; Chu, C.-S.; Shih, C.-H.; Lin, C.-Y.; Huang, K.-T.; Chen, S.-J.; Shu, S.-F. High-efficiency electro-optic polymer light modulator based on waveguide-coupled surface plasmon resonance. In *Plasmonics: Metallic Nanostructures and Their Optical Properties*; International Society for Optics and Photonics: Bellingham, DC, USA, 2003; Volume 5211, pp. 197–206.
29. Gryczynski, I.; Malicka, J.; Nowaczyk, K.; Gryczynski, Z.; Lakowicz, J.R. Waveguide-modulated surface plasmon-coupled emission of Nile blue in poly(vinyl alcohol) thin films. *Thin Solid Films* **2006**, *510*, 15–20. [[CrossRef](#)] [[PubMed](#)]
30. Calander, N. Surface Plasmon-Coupled Emission and Fabry-Perot Resonance in the Sample Layer: A Theoretical Approach. *J. Phys. Chem. B* **2005**, *109*, 13957–13963. [[CrossRef](#)] [[PubMed](#)]
31. Salamon, Z.; Macleod, H.A.; Tollin, G. Coupled Plasmon-Waveguide Resonators: A New Spectroscopic Tool for Probing Proteolipid Film Structure and Properties. *Biophys. J.* **1997**, *73*, 2791–2797. [[CrossRef](#)]
32. Salamon, Z.; Tollin, G. Optical Anisotropy in Lipid Bilayer Membranes: Coupled Plasmon-Waveguide Resonance Measurements of Molecular Orientation, Polarizability, and Shape. *Biophys. J.* **2001**, *80*, 1557–1567. [[CrossRef](#)]
33. Toyama, S.; Doumae, N.; Shoji, A.; Ikariyama, Y. Design and fabrication of a waveguide-coupled prism device for surface plasmon resonance sensor. *Sens. Actuat. B Chem.* **2000**, *65*, 32–34. [[CrossRef](#)]
34. Song, B.; Jiang, Z.; Liu, Z.; Wang, Y.; Liu, F.; Cronin, S.B.; Yang, H.; Meng, D.; Chen, B.; Hu, P.; et al. Probing the Mechanisms of Strong Fluorescence Enhancement in Plasmonic Nanogaps with Sub-nanometer Precision. *ACS Nano* **2020**, *14*, 14769–14778. [[CrossRef](#)]
35. Cao, S.-H.; Cai, W.-P.; Liu, Q.; Xie, K.-X.; Weng, Y.-H.; Huo, S.-X.; Tian, Z.-Q.; Li, Y.-Q. Label-Free Aptasensor Based on Ultrathin-Linker-Mediated Hot-Spot Assembly to Induce Strong Directional Fluorescence. *J. Am. Chem. Soc.* **2014**, *136*, 6802–6805. [[CrossRef](#)] [[PubMed](#)]
36. Li, B.; Ju, H. Label-free optical biosensors based on a planar optical waveguide. *Biochip J.* **2013**, *7*, 295–318. [[CrossRef](#)]
37. Tran, N.H.T.; Phan, B.T.; Yoon, W.J.; Khym, S.; Ju, H. Dielectric metal-based multilayers for surface plasmon resonance with enhanced quality factor of the plasmonic waves. *J. Electron. Mater.* **2017**, *46*, 3654–3689. [[CrossRef](#)]
38. Michal, T.; Joerg, E.; Thomas, R.; Colette, M.; Brian, D.M. Experimental and theoretical evaluation of surface plasmon-coupled emission for sensitive fluorescence detection. *J. Biomed. Opt.* **2008**, *13*, 054021.
39. Venkatesh, S.; Sai Sathish, R. Purcell Factor: A Tunable Metric for Plasmon-Coupled Fluorescence Emission Enhancements in Cermet Nanocavities. *J. Phys. Chem. C* **2016**, *120*, 2908–2913.
40. Kaushal, S.; Nanda, S.S.; Yi, D.K.; Ju, H. Effects of Aspect Ratio Heterogeneity of an Assembly of Gold Nanorod on Localized Surface Plasmon Resonance. *J. Phys. Chem. Lett.* **2020**, *11*, 5972–5979. [[CrossRef](#)] [[PubMed](#)]
41. Lakowicz, J.R. Effects of Solvents on Fluorescence Emission Spectra. In *Principles of Fluorescence Spectroscopy*; Plenum Press: New York, NY, USA, 1983; pp. 187–215.